Application of the projected Landweber method to the estimation of the source time function in seismology

1997 Inverse Problems 13 465

(http://iopscience.iop.org/0266-5611/13/2/017)

Inverse Problems **13** (1997) 465–486. Printed in the UK PII: S0266-5611(97)76475-X

Application of the projected Landweber method to the estimation of the source time function in seismology

M Bertero†, D Bindi†, P Boccacci†, M Cattaneo‡, C Eva‡ and V Lanza‡

† INFM and Dipartimento di Fisica, Università di Genova, Genova, Italy

‡ Dipartimento di Scienze della Terra, Università di Genova, Genova, Italy

Received 12 July 1996, in final form 31 October 1996

Abstract. The empirical Green function (EGF) model, which is used in this paper for the analysis of the waveforms of low-energy earthquakes, consists in assuming that the propagating medium and the recording instrument can be treated as a linear system and that the impulse response function of the system can be approximated by the waveform of a very small earthquake. The deconvolution of the Green function event from the waveform of a larger one, located at approximately the same position, provides information about the source time function (STF) of the latter. Linear inversion methods do not yield satisfactory estimations of the STF which must be positive and causal. Moreover, an estimate of the duration (support) of the STF should be desirable. In this paper we apply to this problem the so-called projected Landweber method, which is an iterative nonlinear method allowing for the introduction of constraints on the solution. The implementation of the method is easy and efficient. We first validate the method by means of synthetic data, generated by the use of waveforms of a seismic swarm that occurred in the Ligurian Alps (north-western Italy) during July 1993. Then, taking into account the indications provided by the simulations, the method has been applied to the inversion of real data, yielding satisfactory results also in the case of quite complex events.

1. Introduction

The waveform generated by an earthquake can be modelled as the convolution of a function characterizing the source, the so-called *source time function* (STF), and a Green function describing the propagation of the seismic wave. If $u^{(0)}(t; P_1)$ is the waveform at the point P_1 on the surface of the Earth, $f^{(0)}(t; P_0)$ the STF of the earthquake at the point P_0 and $G^{(0)}(t; P_1, P_0)$ the Green function of the problem, then

$$u^{(0)}(t; P_1) = \int_{-\infty}^{+\infty} G^{(0)}(t - t'; P_1, P_0) f^{(0)}(t'; P_0)\, \mathrm{d}t'. \tag{1}$$

This relation is based on several approximations. In particular, it is assumed that conditions for far-field approximation (signal wavelength much smaller than P_0P_1-distance) and for Fraunhofer approximation (source dimension much smaller than P_0P_1-distance) are fulfilled.

We point out that equation (1) must satisfy the causality condition. If $u^{(0)}(t; P_1)$ has been shifted in time to correct the time delay between the outset of the event in P_0 and the arrival of the wave in P_1, then the condition $f^{(0)}(t'; P_0) = 0$ for any $t' < t_0$ has to imply that also $u^{(0)}(t; P_1) = 0$ for any $t < t_0$. This causality condition holds true if and only if

$$G^{(0)}(t; P_1, P_0) = 0 \qquad \forall t < 0. \tag{2}$$

0266-5611/97/020465+22$19.50

The use of equation (1) for estimating the STF of an earthquake from an observed waveform requires the knowledge of the Green function. However, the theoretical computation of $G^{(0)}(t; P_1, P_0)$ is, in general, of poor accuracy even at regional distances because wave propagation strongly depends on the spatial variation of elastic rock parameters which, in most cases, are not sufficiently well known. Moreover, the observed waveform is also affected by the site and instrument response.

An approach often used in practice for avoiding these difficulties is the following. If a relatively small earthquake having approximately the same focal mechanism and the same location as a larger event has been observed, then the recorded seismogram of the small event can be used as an approximation of the unknown Green function [1]. This approximation, which also includes the effects of the site and instrument response, is usually called the *empirical Green function* (EGF). Then, if we denote by $G(t)$ the EGF (in the following we omit for simplicity the indication of the points P_0, P_1) and by $u(t)$ the recorded waveform corrupted by a noise term $w(t)$, the basic equation of the EGF model, fulfilling the causality condition, is as follows:

$$u(t) = \int_{-\infty}^{t} G(t - t') f^{(0)}(t') \, \mathrm{d}t' + w(t). \tag{3}$$

The term $w(t)$, which describes the site and instrument noise, is not known but, if $f^{(0)}(t') = 0$ for any $t' < t_0$, then $u(t) = w(t)$ for any $t' < t_0$. Therefore, if $w(t)$ is the realization of a stationary process, its statistical properties can be deduced by an observation of the record of the instrument before the arrival of the signal.

Equation (3) has been widely used for the synthesis of seismograms [2, 3] as well as for the estimation of source parameters and rupture characteristics of both small [4, 5] and large size events [6, 7]. To this purpose one has to recover the STF $f^{(0)}(t)$ from the recorded seismogram $u(t)$ and the EGF $G(t)$. Since in the frequency domain equation (3) becomes

$$\hat{u}(\omega) = \hat{G}(\omega) \hat{f}^{(0)}(\omega) + \hat{w}(\omega) \tag{4}$$

by neglecting the noise term $\hat{w}(\omega)$ one obtains an estimate of $\hat{f}^{(0)}(\omega)$ given by

$$\hat{f}(\omega) = \frac{\hat{u}(\omega)}{\hat{G}(\omega)}. \tag{5}$$

It is well known that $\hat{f}(\omega)$ differs from $\hat{f}^{(0)}(\omega)$ by the noise contribution $\hat{w}(\omega)/\hat{G}(\omega)$ and that this term can be very large at the frequencies corresponding to small values of $\hat{G}(\omega)$. As a consequence, the estimate $f(t)$ obtained by means of the inverse Fourier transform of $\hat{f}(\omega)$ is not reliable. This remark is simply a restatement of the ill-posedness of a deconvolution problem.

A form of regularization has already been used in [4–7] for solving this particular problem. In fact the most frequently used method in seismology is the so-called *water-level method* [8] which consists of introducing a threshold value γ and in considering the function $\hat{G}_\gamma(\omega)$ defined as follows:

$$\hat{G}_\gamma(\omega) = \begin{cases} \hat{G}(\omega) & \text{if } |\hat{G}(\omega)| > \gamma \\ \gamma & \text{if } |\hat{G}(\omega)| \leqslant \gamma. \end{cases} \tag{6}$$

In general, the value of γ is chosen in such a way that the ratio between the maximum value of $\hat{G}(\omega)$ and γ ranges between 20 and 60 dB. Then an estimate of $\hat{f}^{(0)}(\omega)$ is given by

$$\hat{f}_\gamma(\omega) = \frac{\hat{u}(\omega)}{\hat{G}_\gamma(\omega)}. \tag{7}$$

The water-level method contains a rather crude form of regularization and, in practice, it provides results similar to those which can be obtained by means of standard regularization methods such as the Tikhonov, Landweber or conjugate gradient method. Nevertheless, the estimates of the STF obtained by means of these methods show improbable long-period trends and short-period oscillations. Besides, they very often take negative values which make their interpretation difficult, since only a non-negative (unipolar) STF is physically reasonable for 'no back-slip' rupture processes. In order to avoid some of these difficulties, methods based on the approximation of the STF by means of a superposition of pseudo-triangular functions [9] or based on simulated annealing [10] have been proposed.

The problem outlined above, even if rather simple in principle, deserves consideration for two reasons:

(i) the use of constraints on the solution seems to be unavoidable if one wants to get a reliable estimate of the STF;

(ii) the convolution operator is only approximately known (sometimes several approximations of the same operator are available) and the effect of this approximate knowledge on the data inversion should be understood.

In this paper we investigate the effects of the following constraints on the estimation of the STF:

- non-negativity of the STF, i.e. $f(t) \geqslant 0$;
- causality of the STF, i.e. $f(t) = 0$ for $t \leqslant 0$;
- finite duration of the STF, i.e. $f(t) = 0$ for $t > T$, where T is a time interval shorter than the length of the record.

As concerns the last constraint we observe that an *a priori* value of T is not known. We will propose a method for estimating T by performing several inversions corresponding to different values of T. In fact an estimate of T is not only useful information for the observed earthquake; its use in the inversion algorithm can also provide an improvement on the estimate of the STF. In the case of image restoration this effect is known as *super-resolution* and is due to the possibility of extrapolating the Fourier transform of a band-limited image when the support of the image is known [11].

The method we use for taking into account the constraints outlined above is the so-called *projected Landweber method*. It is an iterative method for approximating the solution of constrained least-squares problems [12]. As far as we know, it has not yet been proved that this is a regularization method, even if numerical simulations show that, in general, it has the usual semiconvergence property of the regularizing iterative methods: the restoration error decreases first and increases afterwards, i.e. the restoration error has a minimum corresponding to a certain value of the number of iterations.

As we show in section 2 this method can be easily implemented for the problem considered in this paper. In general, the practical difficulty is that the convergence of the method is too slow and, for this reason, the possibility of accelerating the method by the use of preconditioning has been investigated [13]. In the present paper, however, we do not need this technique because the number of iterations required is moderate, of the order of 100. Moreover, the slow convergence can have a practical advantage, because it implies that the choice of the optimum number of iterations is not very critical.

In section 3 we describe both the real and the synthetic data we use in this paper. In particular, we provide three EGFs and two larger size events for three different stations. The synthetic seismograms are generated by convolving one of the EGFs with Gaussian pulses and by adding to the results the noise affecting the recording of the EGF before the arrival of the P-wave. These synthetic data are used in section 4 for investigating both the effects of the constraints and the effect of the use of an approximate EGF. An interesting

result is the following. If we deconvolve the data by means of the same EGF used for their generation, then we find that the addition of constraints improves considerably the quality of the restored STF and that the residual is always of the order of the noise affecting the data. In particular, we find that the constraints allow for a correct restoration of the Fourier transform of the STF at low frequencies. This information is not contained in the data because a low-frequency cut-off is introduced for removing microseismic noise (see section 2). On the other hand, when we deconvolve the data by means of one of the two other EGFs, the addition of constraints still improves the quality of the restored STF but the residual increases. In other words, we get rather satisfactory estimates of the STF but these estimates do not fit the data. We believe that this behaviour can be used as a criterion for evaluating the accuracy of the EGF. Finally, in section 5 we apply the method to real data and we propose a method for estimating the support of the STF. We show that it is possible to obtain satisfactory results also in the case of quite complex events.

2. The projected Landweber method

If the outset of the event occurs at the time $t = 0$, then $f^{(0)}(t) = 0$ for $t < 0$. The same property holds true for the EGF $G(t)$, see equation (2), and therefore equation (3) implies that it holds true also for $u(t)$, except for the noise term $w(t)$. Functions which are zero for $t < 0$ are called *causal functions*. If we take into account this property and if we omit the noise term, then equation (3) can be written as an ordinary convolution equation for an estimate f of the STF $f^{(0)}$

$$u = G * f \tag{8}$$

where the $*$ denotes the usual convolution product

$$(G * f)(t) = \int_{-\infty}^{+\infty} G(t - t')\, f(t')\, \mathrm{d}t'. \tag{9}$$

We consider equation (8) in $L^2(\mathbb{R})$ and we assume that $\hat{G}(\omega)$ is bounded, so that equation (9) defines a bounded operator in $L^2(\mathbb{R})$.

As is well known, equation (8) can be diagonalized by means of the Fourier transform. Then it is important to note that the Fourier transform $\hat{f}(\omega)$ of a square-integrable causal function $f(t)$ has rather peculiar mathematical properties: it is the boundary value, in the sense of the L^2-norm, of a function $\hat{f}(z)$, $z = \omega + \mathrm{i}\eta$, which is holomorphic in the half-plane $\eta = \mathrm{Im}(z) < 0$; moreover, there exists a constant c such that

$$\int_{-\infty}^{+\infty} |\hat{f}(\omega + \mathrm{i}\eta)|^2\, \mathrm{d}\omega \leqslant c \tag{10}$$

for any real $\eta < 0$. This property of the Fourier transform is not only a necessary but also a sufficient condition characterizing a causal function $f(t)$. This is one of the many Paley–Wiener theorems [14] characterizing the support of a function in terms of properties of its Fourier transform. Since $G(t)$ is also causal, the support of $\hat{G}(\omega)$ coincides with the real axis and therefore the solution of equation (8) is unique.

It is immediate to see that the estimates of the solution of equation (8) provided by the usual regularization methods do not satisfy the causality condition. For instance, in the case of the Tikhonov regularization method one has [15]

$$\hat{f}_\mu(\omega) = \frac{\hat{G}^*(\omega)}{|\hat{G}(\omega)|^2 + \mu}\, \hat{u}(\omega) \tag{11}$$

where $\hat{f}_\mu(\omega)$ denotes the Fourier transform of the regularized solution $f_\mu(t)$ and $\hat{G}^*(\omega)$ is the complex conjugate of $\hat{G}(\omega)$. In this equation, while $\hat{u}(\omega)$ satisfies the causality condition, the filtering factor

$$\hat{G}_\mu(\omega) = \frac{\hat{G}^*(\omega)}{|\hat{G}(\omega)|^2 + \mu} \tag{12}$$

does not have an analytic continuation in the lower half-plane and therefore it is not the Fourier transform of a causal function. As a consequence, the function $f_\mu(t)$ is also not causal, i.e. the inversion method introduces a non-causal component which is unphysical. We point out that this non-causal component is not an effect of the noise but of the approximation implicit in the inversion method.

The previous criticism applies also to another very well known regularization method, i.e. the iterative method known as the *Landweber method* or *successive approximation method* [15]. In the case of the convolution equation (8), the iterative scheme (in general, initialized with $f_0 = 0$) is as follows,

$$f_{n+1} = f_n + \tau G^{\mathrm{T}} * (u - G f_n) \tag{13}$$

where $G^{\mathrm{T}}(t) = G(-t)$ and τ is the *relaxation parameter* which must satisfy the following conditions:

$$0 < \tau < \frac{2}{\hat{G}^2_{\max}} \qquad \hat{G}_{\max} = \sup_\omega |\hat{G}(\omega)|. \tag{14}$$

A suitable choice of τ can be $\tau = 1/\hat{G}^2_{\max}$.

It is well known that the iterative process (13) is equivalent to a filtering because, in the case $f_0 = 0$, one can prove that [15]

$$\hat{f}_n(\omega) = \hat{G}^{(n)}(\omega)\hat{u}(\omega) \tag{15}$$

where

$$\hat{G}^{(n)}(\omega) = [1 - (1 - \tau|\hat{G}(\omega)|^2)^n]\frac{1}{\hat{G}(\omega)}. \tag{16}$$

Again this filter function does not have an analytic continuation in the lower half-plane and therefore the regularized solution $f_n(t)$ provided by equation (15) is not causal. It is possible to show, by means of numerical examples, that the Landweber method provides results quite similar to those obtained by means of the water-level method mentioned in the introduction. In fact, all the regularization methods which imply a linear filtering yield similar results once the relevant parameter (water-level γ, regularization parameter μ, number of iterations n, etc) has been properly chosen.

The iterative method (13), however, can be modified in order to introduce constraints on the solution. This modified method is called the *projected Landweber method* (or projected gradient method) and its convergence and regularization properties have been recently investigated [12].

Assume that we know that the solution of the problem (8) must belong to some closed and convex set $\mathcal{C}$. Then the modification of the iterative scheme (13) is as follows,

$$f_{n+1} = \mathcal{P}_\mathcal{C}[f_n + \tau G^{\mathrm{T}} * (u - G * f_n)] \tag{17}$$

where $\mathcal{P}_\mathcal{C}$ denotes the convex projection (or metric projection) onto the closed and convex set $\mathcal{C}$. In general, also this iteration scheme is initialized by taking $f_0 = 0$. The convergence

result is as follows [12]: in the absence of noise f_n converges (weakly) to the constrained least-squares solution, i.e. the unique solution $\tilde{f}_{\mathcal{C}}$ of the following problem:

$$\|G * f - u\| = \text{minimum} \qquad f \in \mathcal{C}. \tag{18}$$

The uniqueness of the solution of this problem follows from the injectivity of a causal convolution operator. The problem, however, can still be ill-posed as concerns existence and continuity of the solution.

In the case of equation (8), the appropriate closed and convex set for the STF is *the set of non-negative causal functions which are zero for* $t > T$, where T is a time interval shorter than the duration of the recorded seismogram. The value of T is not known but it can be used as a free parameter in the data inversion.

It is very easy to show that the projection operator $\mathcal{P}_{\mathcal{C}}$ onto the previous closed and convex set is defined as follows:

$$(\mathcal{P}_{\mathcal{C}} f)(t) = \begin{cases} f(t) & \text{if } f(t) > 0 \text{ and } 0 < t < T \\ 0 & \text{elsewhere.} \end{cases} \tag{19}$$

Therefore, this projection operator can be easily computed. However, since we will investigate the effect of the various constraints on inversion, we will also use the following projections: the projection $\mathcal{P}_+$ on the closed and convex set of the non-negative functions

$$(\mathcal{P}_+ f)(t) = \begin{cases} f(t) & \text{if } f(t) > 0 \\ 0 & \text{if } f(t) \leqslant 0 \end{cases} \tag{20}$$

the orthogonal projection $\mathcal{P}_c$ on the linear subspace of causal functions

$$(\mathcal{P}_c f)(t) = \begin{cases} f(t) & \text{if } t \geqslant 0 \\ 0 & \text{if } t < 0 \end{cases} \tag{21}$$

and the orthogonal projection $\mathcal{P}_{\mathcal{T}}$ on the linear subspace of the functions which are zero for $t > T$

$$(\mathcal{P}_{\mathcal{T}} f)(t) = \begin{cases} f(t) & \text{if } t \leqslant T \\ 0 & \text{if } t > T. \end{cases} \tag{22}$$

It is easy to verify that these operators commute and that the operator $\mathcal{P}_{\mathcal{C}}$ of equation (19) is given by $\mathcal{P}_{\mathcal{C}} = \mathcal{P}_+ \mathcal{P}_c \mathcal{P}_{\mathcal{T}}$. Moreover, we will also use the operators $\mathcal{P}_+$ (constraint of non-negativity) and $\mathcal{P}_+ \mathcal{P}_c$ (constraint of non-negativity and causality). For all these operators the implementation of the iterative method (17) is easy.

We start with $f_0 = 0$. Then, given $f_n(t)$, by means of its Fourier transform $\hat{f}_n(\omega)$ (which, in the case of discretized functions can be computed by means of the FFT algorithm) one computes the function

$$\hat{g}_{n+1} = \hat{f}_n(\omega) + \tau \hat{G}^*(\omega)[\hat{u}(\omega) - \hat{G}(\omega)\hat{f}_n(\omega)]. \tag{23}$$

The inverse Fourier transform $g_{n+1}(t)$ of $\hat{g}_{n+1}(\omega)$ is computed and the new approximation $f_{n+1}(t)$ is obtained by projecting $g_{n+1}(t)$ by means of the appropriate projection operator ($\mathcal{P}_+$ or $\mathcal{P}_+ \mathcal{P}_c$ or $\mathcal{P}_+ \mathcal{P}_c \mathcal{P}_{\mathcal{T}}$). Therefore, at each iteration, the algorithm requires the computation of one direct and one inverse Fourier transform, followed by a projection operation. It is obvious that the total number of operations is of the order of $2N \ln N$ if N is the total number of points in the seismogram. Moreover, if we perform K iterations, the total number of operations will be of the order of $2KN \ln N$.

Finally a few words about the stopping rules for the iterative process. In the case of the convex set $\mathcal{C}$ considered for the STF, the problem (18) is still ill-posed and therefore one has

to stop the iterative process in order to get a regularized approximation of the constrained least-squares solution. As far as we know, no criterion has been established for the method we are considering in this paper. From numerical simulations which will be described in section 4, it follows that the iterates f_n first approach the true solution and then go far away. Therefore, it is necessary to stop the procedure and this point will be discussed in the following sections.

3. Description of the data used for the validation of the method

North-western Italy is characterized by a seismicity of relatively low level (on a global scale) but nevertheless quite frequent and diffuse. Since 1982, a regional network (IGG network, Genova, Italy) of telemetered short period stations, equipped with vertical component seismometers with a natural frequency of 1 Hz, has continuously monitored this area [16]. From most stations, the analogue signals are transmitted by FM links to the central recording site: this operation introduces both a dynamic range limitation (around 66 dB) and a bandwidth reduction (0.2–20 Hz). At the central recording site the signals are non-stop digitized by a high dynamic system and radio-synchronized on a DCF signal with a smoothing technique, assuring a time stability better than 1 ms; the sampling rate is about 13 ms (corresponding to a cut-off frequency of about 38 Hz).

Data used in this work belong to a seismic swarm which occurred in the Ligurian Alps during July 1993. More than 600 events were located by the regional and temporary networks, showing that most hypocentres are confined to a volume of a few km^3 (see figure 1). The strong coherency of the signals recorded by the same station (evaluated by means of the maximum peak of normalized cross correlation) confirms the striking contiguity of the hypocentral solutions and allows one to think that the focal mechanism has not significantly changed during the whole swarm. With such characteristics (i.e. same source–receiver path and focal mechanism for most events), these events seem very suitable for testing the deconvolution method described in the previous section.

The waveforms of three small earthquakes have been used as the EGF while we have selected two mainshocks with different characteristics: one with a behaviour of the waveform similar to that of the EGF (simple event), the other with a rather different structure (complex event). The hypocentral coordinates and magnitudes of the selected events are presented in table 1. The three EGFs are indicated with the numbers 42, 46 and 48; the simple event has the number 2932, while the complex one has the number 5139. Moreover, among all the recordings of the network those of the stations PCP, ROB and IMI (see figure 1) have been selected because of their very high signal-to-noise ratio (about 60 dB).

Table 1. Hypocentre parameters for the events used. M_D and M_L are for duration and local magnitude, respectively.

Event	Origin time (y m-d h-m-s)	Latitude (deg min)	Longitude (deg min)	Depth (km)	Magnitude	
					M_D	M_L
MAIN2932	93 0714 232932.2	44N13.6	8E14.8	7	3.0	2.7
MAIN5139	93 0717 115139.3	44N12.9	8E15.0	8	3.3	3.0
EGF42	93 0715 003143.0	44N13.9	8E15.0	6	2.4	1.8
EGF46	93 0716 014827.1	44N13.5	8E15.8	7	2.3	1.7
EGF48	93 0714 234939.1	44N14.2	8E14.6	6	2.1	1.6

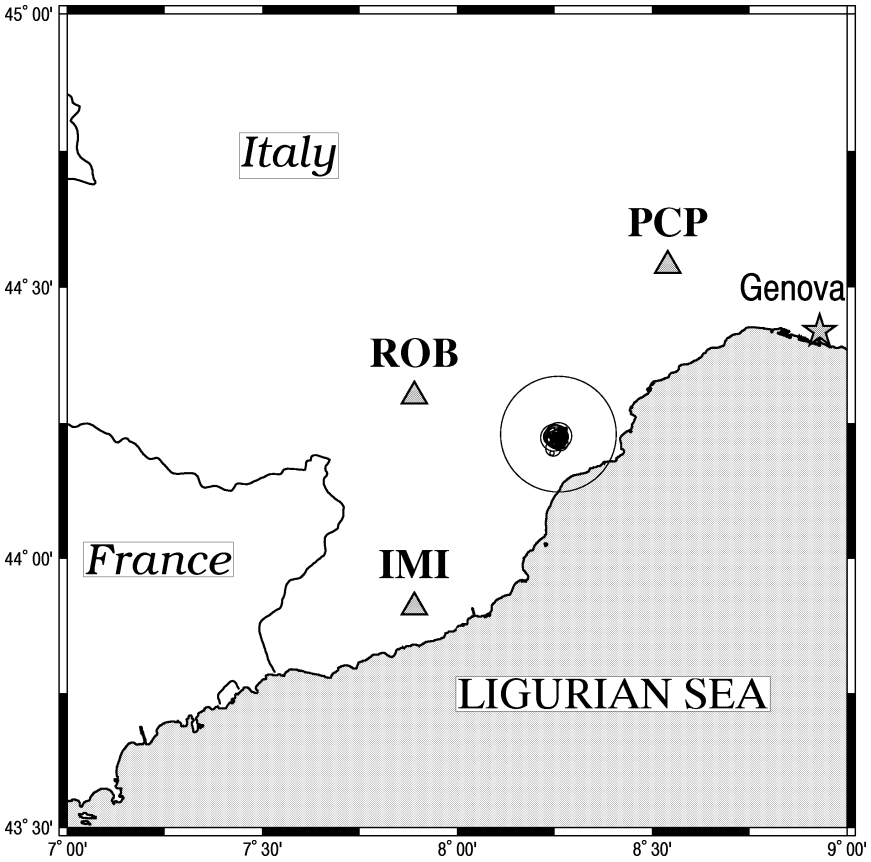

Figure 1. Map of the position of the events which occurred during the sequence of July 1993. The circle limits the region of interest. The triangles correspond to the three stations of the IGG network used in this work.

The 15 waveforms considered have been interpolated by means of sinc-functions corresponding to the frequency of 38 Hz and have been resampled at the rate of 5 ms (corresponding to a frequency of 100 Hz). This oversampling has been chosen in order to improve both the estimate of the very first onset of the P waveform and the estimate of the main features of the deconvolved STF (e.g. rupture duration). In order to remove the frequencies introduced by the resampling, the signals were filtered with a second-order Butterworth band-pass filter with a band-pass between 1 and 20 Hz. The cut-off at low frequencies is introduced in order to remove the microseismic noise affecting all the traces. Finally, the P waveforms were windowed to a length of about 1 s. The records are presented in figure 2. We point out that the EGF42, especially in the time interval corresponding to the first 100 samples, is quite similar to the MAIN2932 for all the three stations we have considered. Moreover, the EGF48 is similar to the EGF42 for the stations ROB and PCP while it is rather different for the station IMI. Finally, the EGF46 has an opposite behaviour: it is similar to the EGF42 for the station IMI and rather different for the other two stations.

The length of each record is about 200 samples (corresponding to a duration of about 1 s). In order to take into account causality and also to avoid the recovering effects due to cyclic convolutions, the records have been padded by zeros so that the total length is

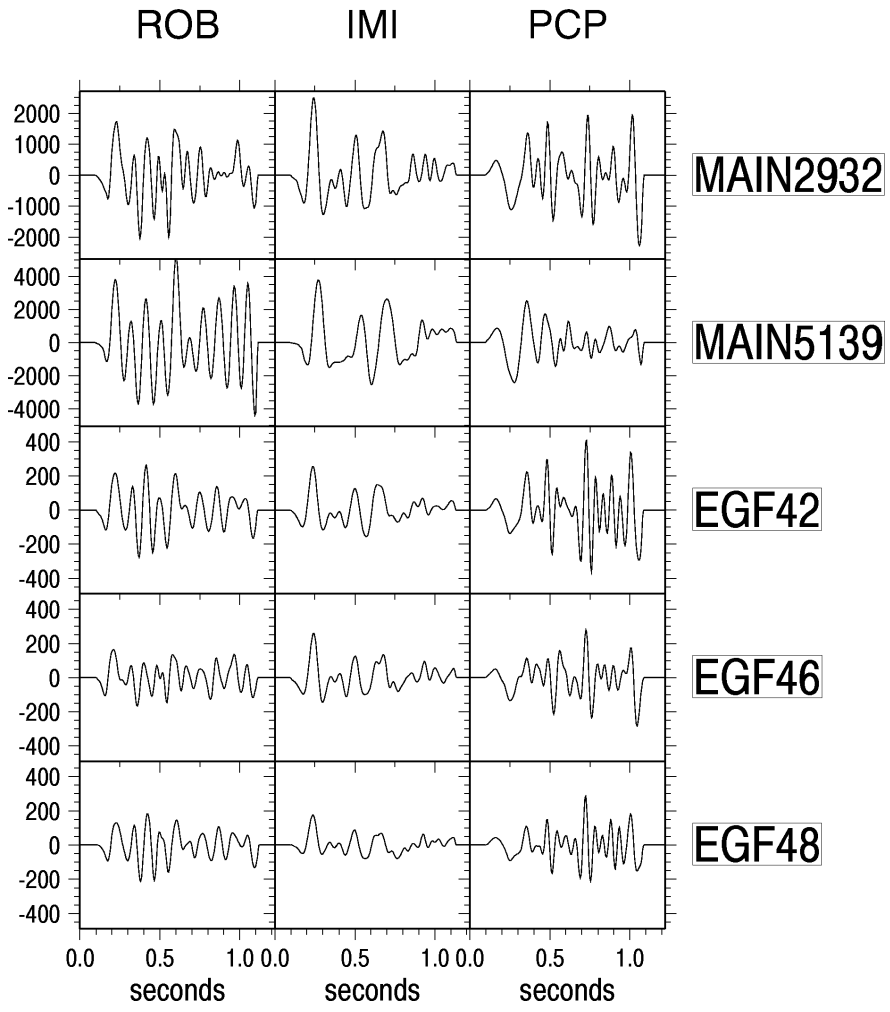

Figure 2. Waveforms (in arbitrary units) of the P-wave portion of the two mainshocks (MAIN2932 and MAIN5139) and of the three EGFs (EGF42, EGF46 and EGF48) used. The recording stations are indicated at the top of the columns while event identification codes are listed at the right of each row.

512 samples. The records are aligned in such a way that the arrival time corresponds to the same sampling point for each record. However, the uncertainty in the estimation of the arrival time is about 30 ms corresponding to about six samples. For this reason we will leave this uncertainty when applying the constraint of causality.

In order to validate the deconvolution method by means of simulations, we have also generated synthetic waveforms. We have considered four STF having a Gaussian shape

$$f(t) = \begin{cases} A \exp\left(-\dfrac{t^2}{2\sigma^2}\right) & \text{if } f(t) \geqslant A/100 \\ 0 & \text{elsewhere} \end{cases} \tag{24}$$

with a width σ of 25, 20, 15 and 10 ms, corresponding to 5, 4, 3 and 2 samples, respectively. For each Gaussian the amplitude A has been computed in such a way that the four STF have

the same area, i.e. the same relative seismic moment, with a value typical of a small energy mainshock ($M_L \simeq 3$). The Fourier transform of the first two Gaussians is concentrated inside the band of 20 Hz, the Fourier transform of the third one has a small tail between 20 and 30 Hz while the last one has a large tail between 20 and 40 Hz.

The STFs above have been convolved with EGF42 and waveforms with a causal behaviour have been obtained. The non-zero section of the signal has been perturbed by noise obtained from a window of about 1 s on the trace of the EGF (resampled and filtered) a few seconds before the P-wave arrival. Here we assume that the noise is additive and stationary.

4. Results in the case of synthetic data

We have first deconvolved the synthetic waveforms corresponding to Gaussian STFs by means of the same EGF used for generating the data. We have compared the results obtained by means of the water-level method with the results obtained by means of the Landweber method both without and with different kinds of constraints. In fact we have considered the effect of positivity, the effect of positivity plus causality and the effect of positivity plus causality plus finite duration of the STF. In the subsequent tables we will indicate the various methods as follows:

WL = water-level method;

L = Landweber method without constraints;

LP = Landweber method with positivity;

LPC = Landweber method with positivity and causality;

LPCS = Landweber method with positivity plus causality and support constraint.

The condition number of the EGF42, i.e. the ratio between the maximum and minimum value of the modulus of its Fourier transform, is about 10^4 (for all the stations considered). The signal-to-noise ratio of the synthetic data, computed as the ratio between the Euclidean norm of the signal and the Euclidean norm of the noise is about 10^3, i.e. 60 dB. This value is a bit greater than that corresponding to real data.

At each iteration step, if f_n is the result of the nth iteration, we compute the relative discrepancy between the data g and the data computed by means of f_n (i.e. the ratio between the Euclidean norm of the residual and the Euclidean norm of g)

$$\varepsilon_n = \frac{\|Af_n - g\|_2}{\|g\|_2} \tag{25}$$

as well as the relative reconstruction error

$$\delta_n = \frac{\|f_n - f\|_2}{\|f\|_2}. \tag{26}$$

This has been computed both on the full length of the signal (512 samples) and on a region of interest consisting of about 41 samples centred on the maximum of the STF.

We have considered a maximum number of 400 iterations. We report results only in the case of the ROB station because we have obtained similar results for the two other stations.

Behaviour of ε_n. The relative discrepancy is a decreasing function of n (as it follows from theoretical results) and after a few iterations a value of the order of the inverse signal-to-noise ratio is reached. All the methods provide approximately the same value of ε_n, for a given n; however, the methods with more constraints provide smaller values of ε_n (see figure 3(a) in the case $\sigma = 2$). As we will see, this is a behaviour which is opposite to that found when deconvolving with an EGF which is not the correct one.

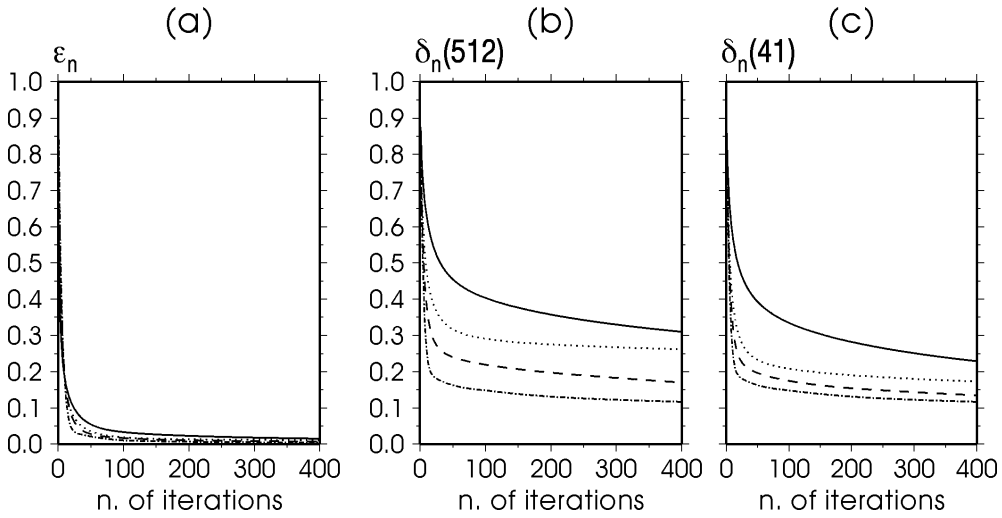

Figure 3. Behaviour, as a function of the number of iterations, of the relative discrepancy ε_n (a) and of the relative reconstruction error δ_n computed on the full length of the signal (b) and on 41 samples centred on the maximum of the STF (c). Plots are relative to the Gaussian with $\sigma = 2$. The four Landweber methods are represented by: full curve, L; dotted curve, LP; dashed curve, LPC; and dash-dotted curve, LPCS (see the text for the explanation of these abbreviations).

Behaviour of δ_n. It is, in general, a decreasing function of n (see figures 3(b) and (c) in the case $\sigma = 2$) even if in the case of the broadest Gaussians a minimum is found for a value of $n < 400$. Since a minimum is expected, this means that the minimum occurs for $n > 400$. However, the minimum is so flat that we do not need so many iterations to obtain a reliable result. More precisely, δ_n is rapidly decreasing for the first iterations but after 100 iterations it does not change significantly. Moreover, for a given n, the value of δ_n decreases when we increase the constraints on the solution.

More quantitative results are provided in figure 4 and in the related tables. We give only results relative to the broadest ($\sigma = 5$) and the narrowest ($\sigma = 2$) Gaussian. We see that the broadest Gaussian, whose Fourier transform is concentrated within the band of the EGF, is perfectly reconstructed by all the constrained methods, but not by the linear methods. In fact the linear methods (water-level and Landweber without constraints) are not able to restore the Fourier transform at low frequencies where information is lacking. This point will be more clear in a moment.

In the tables we give also the values of δ computed for the solution provided by the WL method. These values are even greater than those corresponding to the solutions provided by the L method. We also notice that, in the case of the broadest Gaussian, the use of all the constraints produces an improvement of the overall error by a factor of 25 and of the error on the region of interest by a factor of 15. In the last case the greater part of the improvement is produced by the constraint of positivity. Similar remarks apply to the case of the narrowest Gaussian, even if, of course, the reconstruction error is larger than that of the broadest Gaussian (about 1% for $\sigma = 5$ and about 12% for $\sigma = 2$).

For these reconstructions we have used all the samples where the synthetic waveform is different from zero. This number is obviously larger than the number of non-zero samples of the EGF42. Therefore, in order to simulate what we are doing in practice where, before zero padding, the length of the EGF coincides with the length of the mainshock, we have

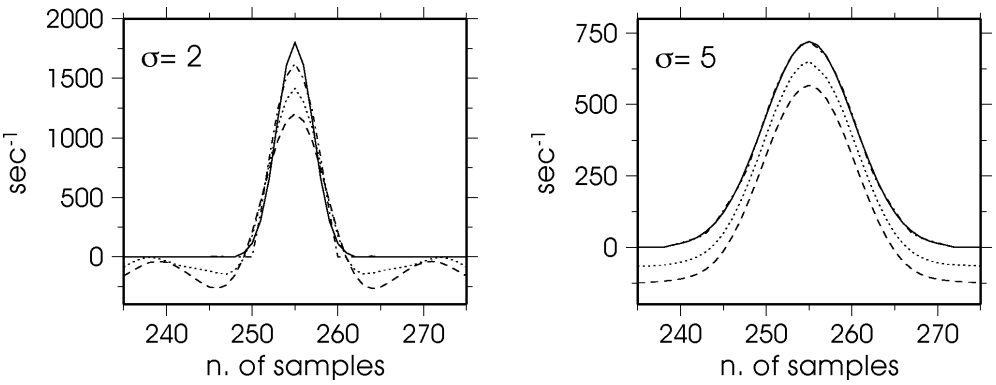

Figure 4. Reconstruction of a Gaussian STF with $\sigma = 2$ (left) and with $\sigma = 5$ (right). In both plots the full curve corresponds to the original Gaussian, the dashed curve to the WL restoration, the dotted curve to the L restoration and the dash-dotted curve to the LPCS restoration.

Table 2. Table relative to figure 4. The values of n, ε and δ are reported for both linear (WL and L) and constrained methods (LP, LPC and LPCS). ε is the quantity defined in (25) with n as given in the second column: $\delta_{(512)}$ is the quantity defined in (26) and computed using all the sampling points while $\delta_{\mathrm{IR}(41)}$ is the same quantity computed using only the 41 sampling points of the region of interest.

	$\sigma = 2$				$\sigma = 5$			
	n	ε	$\delta_{(512)}$	$\delta_{\mathrm{IR}(41)}$	n	ε	$\delta_{(512)}$	$\delta_{\mathrm{IR}(41)}$
WL	—	0.033	0.540	0.370	—	0.041	0.701	0.389
L	400	0.015	0.309	0.228	400	0.017	0.330	0.201
LP	400	0.011	0.261	0.173	400	0.011	0.192	0.016
LPC	400	0.007	0.170	0.135	182	0.004	0.092	0.013
LPCS	400	0.004	0.117	0.117	242	0.003	0.013	0.013

truncated the synthetic waveforms by taking, again before zero padding, only the first 200 samples different from zero. We have found that in the case $\sigma = 2$ the value of δ does not change significantly (it is about 12%) while in the case $\sigma = 5$ the new value of δ is about 10% (the previous one was about 1.3%).

In order to appreciate the improvement obtained by means of the constrained method, it is useful to compare the Fourier transform of the original STF with that of the constrained restoration and that of the water-level restoration. In figure 5 we give the results for all the Gaussian STF we have considered. It is evident that the constrained method yields a good extrapolation of all the STF in the region around $\omega = 0$ and also an extrapolation outside the band of the EGF in the case of the STF with $\sigma = 2$ and $\sigma = 3$. These effects are even more evident in a logarithmic plot given in figure 6 for the cases $\sigma = 2$ and $\sigma = 5$. In both cases the constrained method allows a correct estimation of $\hat{f}(0)$. This quantity, usually denoted by Ω_0 in seismology and called the *low-frequency level*, yields an estimate of the energy of the earthquake, i.e. the seismic moment. As regards the estimation of the corner frequency, one finds the correct value of about 12 Hz for the Gaussian with $\sigma = 5$ and an underestimated value of 25 Hz (in front of a correct value of 30 Hz) in the case of the Gaussian with $\sigma = 2$.

The second part of our numerical experiments consists in deconvolving by the use of

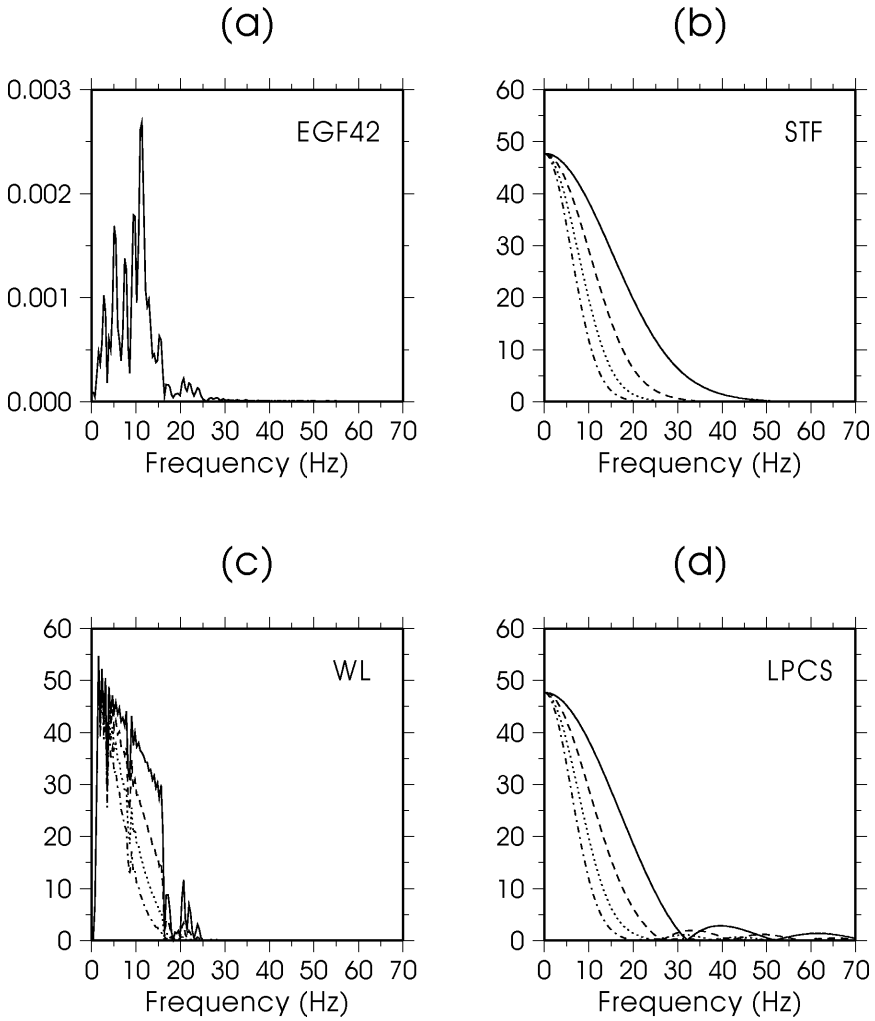

Figure 5. (a) Modulus of the Fourier transform (linear scale) of EGF42; (b) of the original Gaussian STF; (c) of the reconstruction obtained by means of the water-level method; (d) of the reconstruction obtained by means of the constrained method. The full curve corresponds to the narrowest Gaussian ($\sigma = 2$), the dash-dotted curve to the broadest Gaussian ($\sigma = 5$), and dashed and dotted curves are relative to the intermediate ones ($\sigma = 3$ and $\sigma = 4$, respectively).

EGF46 and EGF48 the synthetic data generated by means of EGF42. From figure 2 we see that, in the case of the ROB station, the EGF48 is much more similar to the EGF42 than the EGF46 and therefore we expect to obtain acceptable results by means of EGF48.

In figure 7 we present the behaviour of ε_n and δ_n as functions of n for the deconvolution of the $\sigma = 2$ Gaussian waveform by means of EGF46 and EGF48. The differences with respect to the case of deconvolution by means of the correct EGF are evident, especially in the case of EGF46. We can summarize the main conclusions as follows.

• If we introduce more and more constraints in the deconvolution algorithm, for a given n the values of ε_n increase. This means that, when we use an incorrect model for the deconvolution of the waveform, the introduction of constraints implies that it is not possible

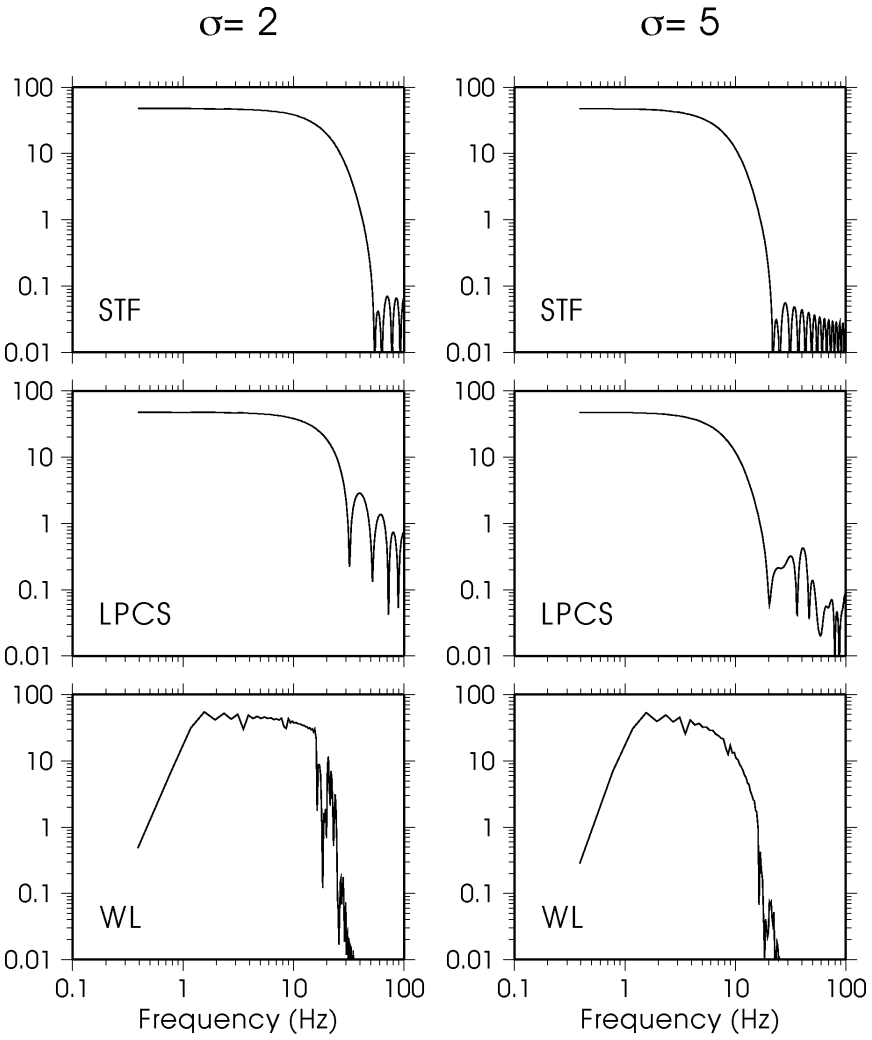

Figure 6. Logarithmic plots of the modulus of the Fourier transform of the STF (top), of the restoration with the constrained method (middle) and of the restoration with the water-level method (bottom) for the cases $\sigma = 2$ (left) and $\sigma = 5$ (right). The side-lobes in the STF are due to the truncation of the Gaussian shape.

to fit the data within experimental errors. An unconstrained method allows a good fit of the data even in the case of an incorrect model but the price to be paid is a completely unreliable restoration. We also see that the effect we are discussing is larger in the case of EGF46 than in the case of EGF48.

• As concerns δ_n the behaviour is opposite with respect to ε_n. The use of constraints improves the quality of the restoration. This result emphasizes the relevance of using constrained methods, even in the case of a poorly correct EGF, for obtaining not completely unreliable results of the deconvolution process. In the case of EGF46 the best value of δ_n we obtain is 40%, while in the case of EGF48 it is 20%. In figure 8 we compare the restoration of the $\sigma = 2$ Gaussian STF, obtained by the use of EGF46, with that obtained by the use of EGF48. This figure clearly shows that large errors in the EGF can introduce

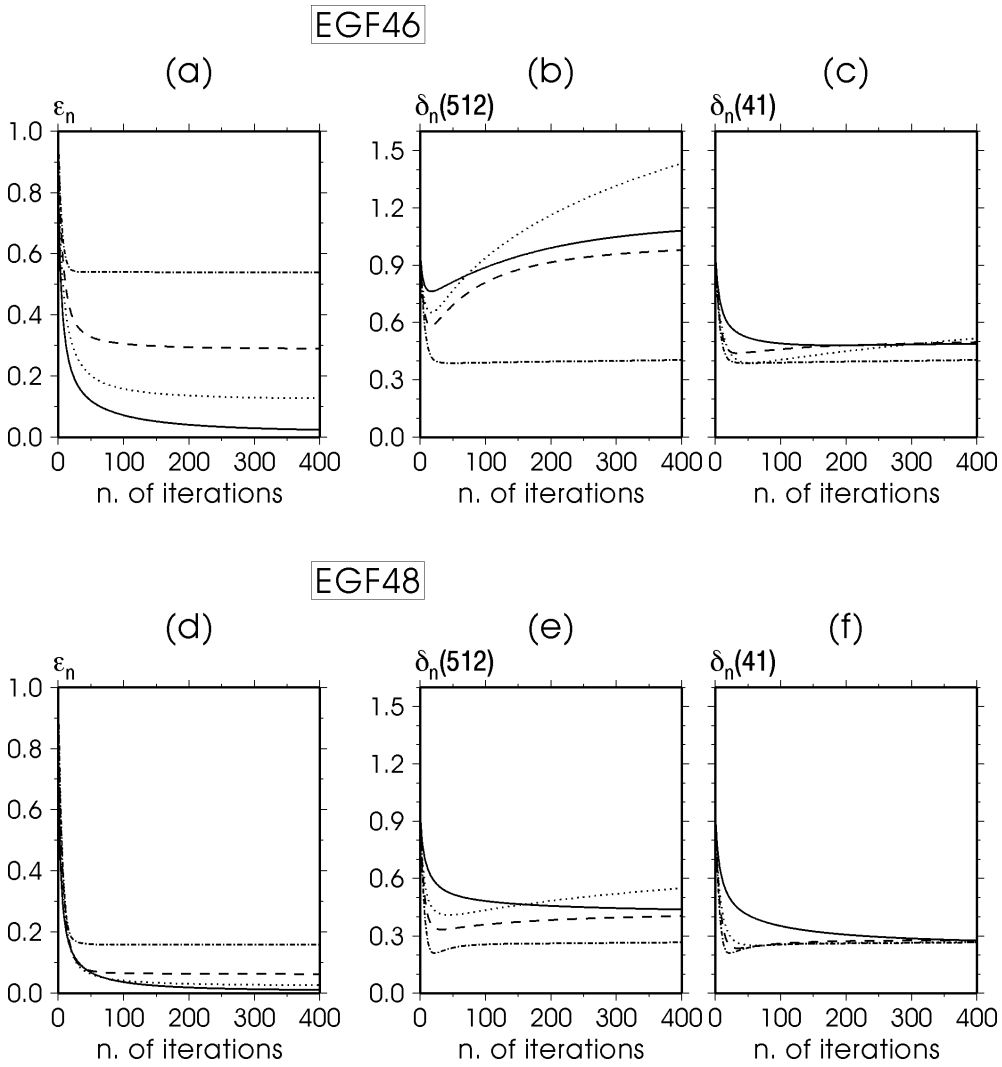

Figure 7. Plots of the relative discrepancy ε_n ((a) and (d)) and of the relative reconstruction error δ_n computed on the full length of the signal ((b) and (e)) and on 41 samples centred on the maximum of the STF ((c) and (f)). Synthetic data, corresponding to the $\sigma = 2$ Gaussian STF, have been deconvolved with the EGF46 (top) and with the EGF48 (bottom). The results of the four Landweber methods are represented by: full curve, L; dotted curve, LP; dashed curve, LPC; and dash-dotted curve, LPCS.

severe distorsion in the restoration of the STF.

• From figure 7 we deduce that the minimum of δ_n occurs for a value of n smaller than 100 (see the remark on the behaviour of δ_n in the case of restorations by the use of the correct EGF). The minimum, however, is rather flat, especially when we use all the constraints on the solution. This is also true in the case of EGF46 (figure 7(b)) even if the minimum is rather deep when not all the constraints are used. For these reasons in the analysis of real data we will use about 100 iterations.

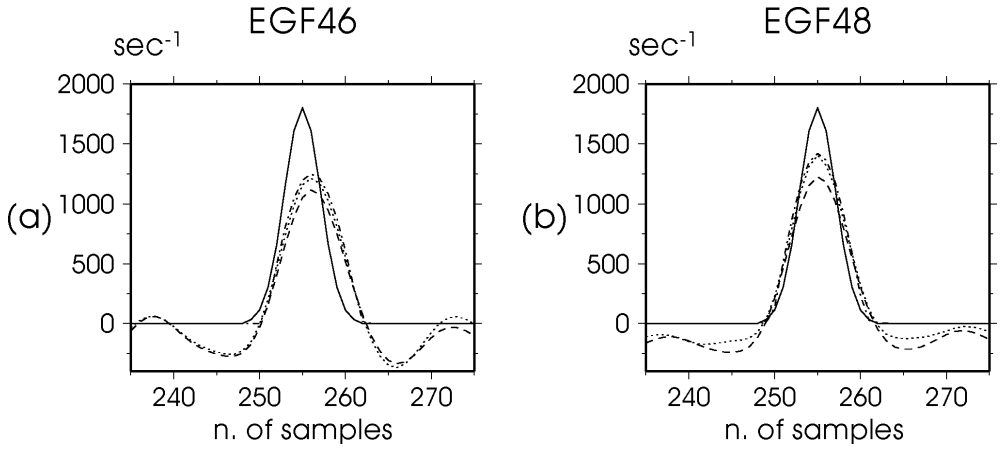

Figure 8. Reconstruction of the STF with $\sigma = 2$ when the synthetic data are deconvolved with EGF46 (left) and with EGF48 (right). In both plots the full curve corresponds to the original Gaussian, the dashed curve to the WL method, the dotted curve to the L method and the dash-dotted curve to the LPCS method.

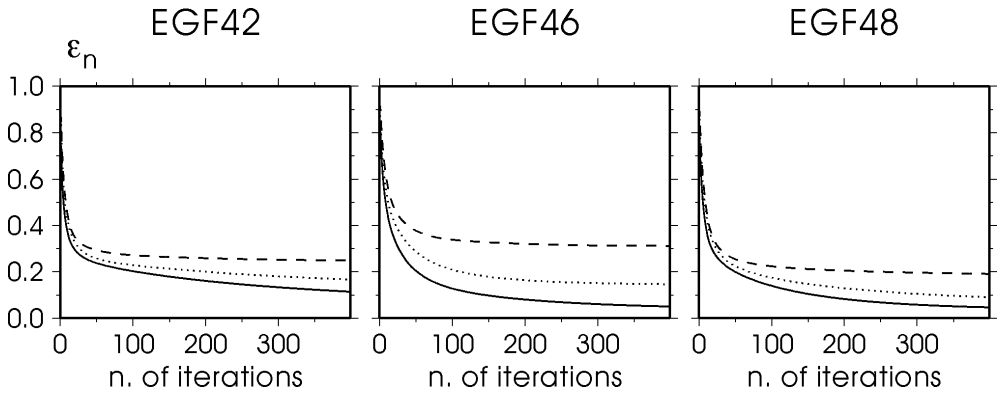

Figure 9. Plots of the relative discrepancy ε_n when the *simple* event (MAIN2932) is deconvolved with the three EGFs. ε_n is computed over the full length of the waveform. Full curves correspond to the L, dotted curves to the LP and dashed curves to the LPC method. Station ROB.

5. Results in the case of real data

The method developed and tested in the previous sections has been applied to the inversion of the two waveforms indicated as MAIN2932 and MAIN5139 in figure 2.

As suggested by the analysis of section 4, we have first investigated the variation of ε_n, equation (25), when we introduce more and more constraints on the solutions. We remember that the analysis with the synthetic data showed that such variation of ε_n is more evident as the EGF differs from the true propagation model. Following these remarks, we look for the EGF, among those at our disposal, whose variation of ε_n is weakly dependent upon the number of constraints. For both mainshocks, the computations have been performed using all the EGFs and all the stations. In the case of MAIN2932 and ROB station, the results are plotted in figure 9. The variation on ε_n due to the addition of constraints is not so large as that plotted in figure 7 in the case of the inversion, by means of EGF46, of

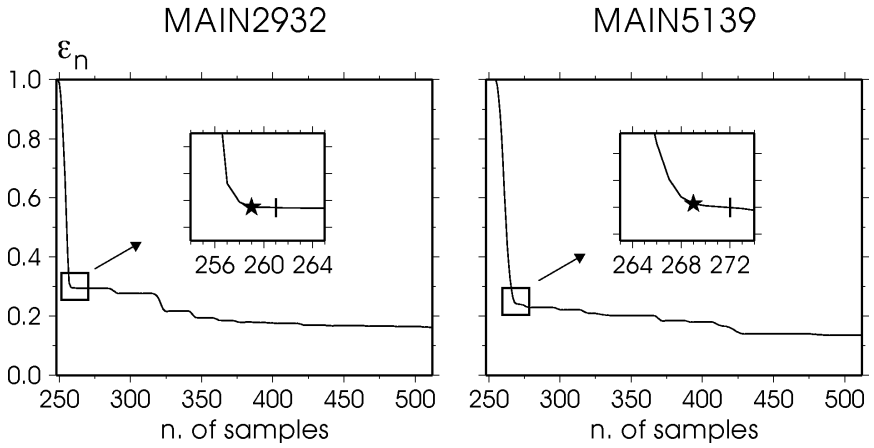

Figure 10. Plots of the relative discrepancy ε_n for $n = 100$ as a function of the number of samples of the STF support. Plots refer to MAIN2932 (left) and to MAIN5139 (right). ε_n is computed on the full length of the waveform. Station IMI. In the small rectangle we indicate the position of the sample used as a right limit of the support in the restorations (vertical bar) and that of the sample just before the steep increase of ε_n (star).

synthetic data generated by means of EGF42. We could conclude that, even if none of the three EGFs is completely correct, nevertheless none is completely wrong. All the results are reported in table 3 for MAIN2932 and in table 4 for MAIN5139. In these tables we give, for the three stations and the three EGF, the values of ε_n, after 400 iterations, both for the unconstrained Landweber method (L) and the projected Landweber method with the constraints of positivity and causality (LPC). The values of ε_n are computed over the full length of the mainshock. Smaller values of the relative discrepancy are obtained if computed over a shorter window of about 100 samples from P-wave onset: in the tables they are reported as ε'_n.

From these tables it clearly appears that the EGF42 is that producing the smallest variations (between L and LPC) both in ε_n and ε'_n for all the stations and for the two events. In most cases it is also the EGF producing the smallest values of ε_n and ε'_n in the constrained case. For these reasons we can consider EGF42 as the best approximation we have for the empirical Green function of these events. In the following we will use EGF42 for our analysis.

The next step is the attempt of estimating the duration of the source function. To this purpose we use the LPCS method with 100 iterations (this number has been estimated in the previous section) and we compute the variation of ε_n when we change the support of the STF. The behaviour is plotted in figure 10. It clearly shows that ε_n slowly increases when we reduce the support of the STF down to a certain value and that it suddenly increases below it. This rather sharp transition seems to provide a quite precise definition of the support of the STF. The estimate of the support obtained in this way and indicated in figure 10 (we use a support a bit broader than that corresponding to the steep increase of ε_n) is used for the estimation of the STF by means of the LPCS method with 100 iterations. In figure 11 we give the results obtained in this way and we compare these results with those obtained by means of the water-level method. We also give the fits of the waveforms provided by the constrained solutions which, at least for the first half of the signal, are quite satisfactory. We see that our method allows for a clear and reliable

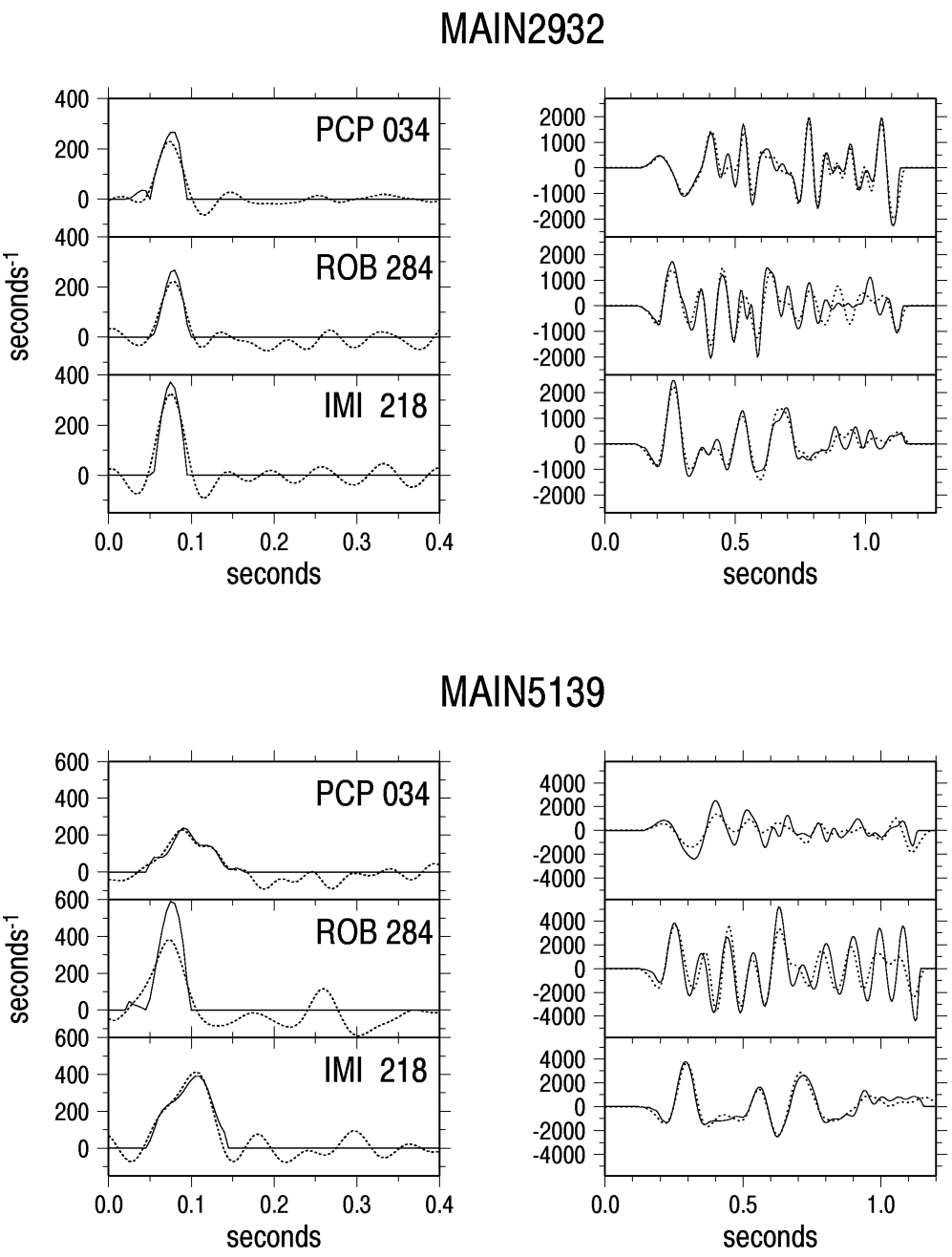

Figure 11. Left: source time functions obtained with the LPCS method (full curve) and with the water-level (dotted curve). Station code and hypocentre–receiver azimuth are indicated. Right: original waveforms (in arbitrary units) of the mainshocks (full curve) and the fits (dotted curve) obtained convolving the used EGF (EGF42 for both mainshocks) with the LPCS solutions.

estimate of the width (T) of the source time function. In contrast the oscillations and the negative parts affecting the STF obtained by means of the water-level method make it hard

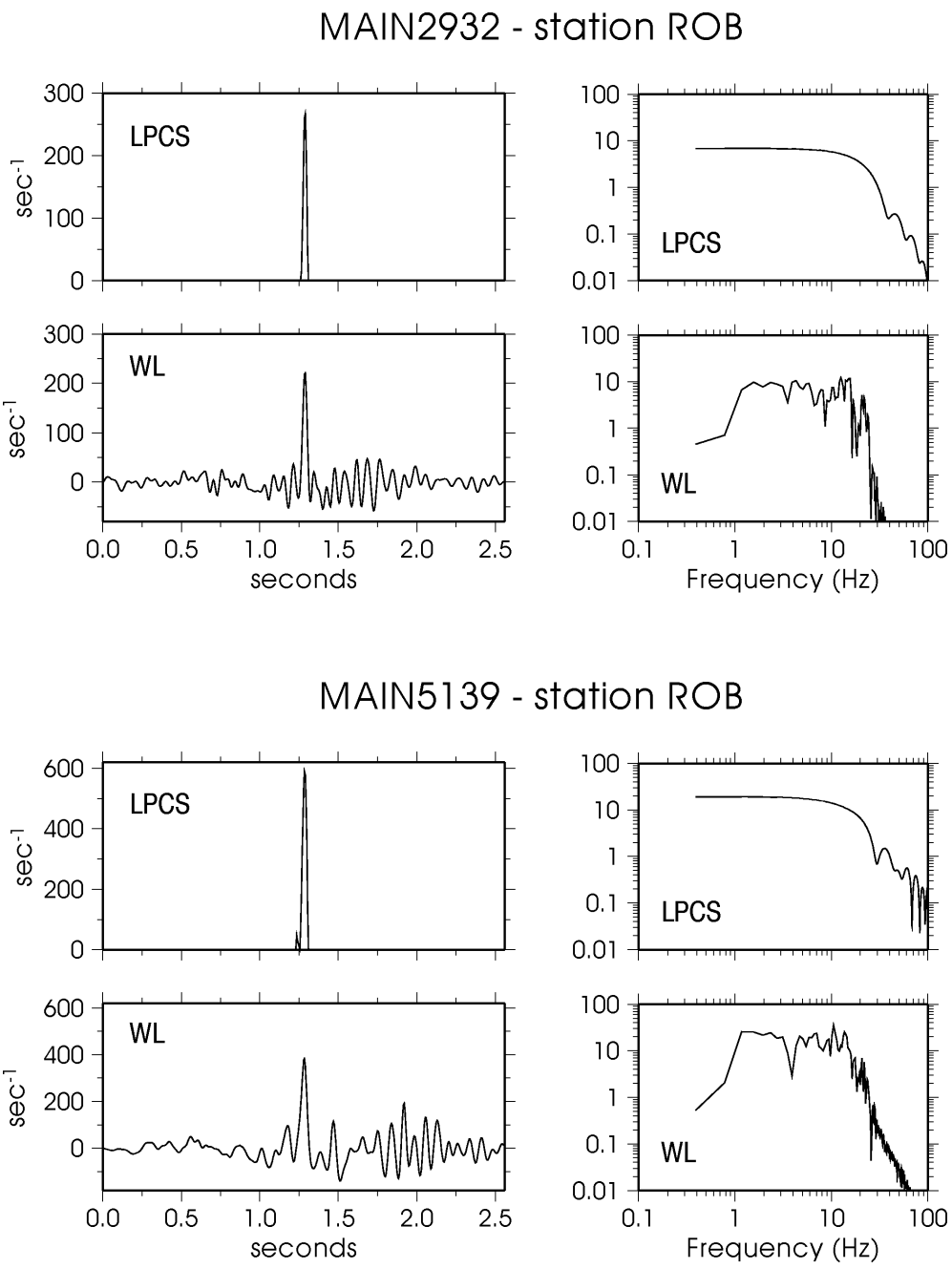

Figure 12. Source time functions (left) and the relative Fourier transforms (right) obtained with the LPCS method (top of each event) and with the water-level method (bottom).

to determine the beginning and the end of the source function. Values of T measured for both the events at the three stations are reported in table 5. We find that the pulse widths of MAIN2932 for stations at different azimuth are almost the same (about 0.05 s). This

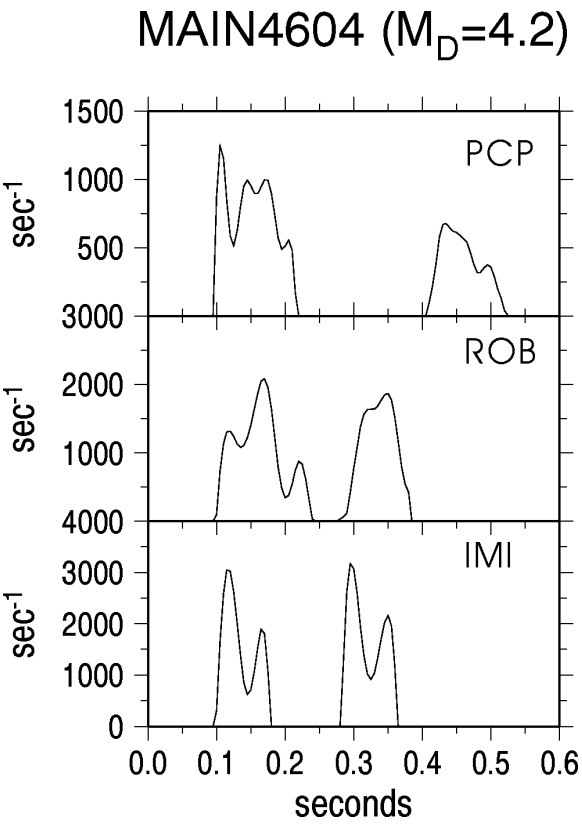

Figure 13. Source time functions of a quite complex earthquake obtained with the LPCS method. The empirical Green function used was EGF48. Two events are clearly recognizable, both consisting of at least two subevents.

Table 3. Results of real data analysis: case of MAIN2932. ε_n is computed over all the support of the mainshock, while ε'_n is computed over a window of 100 samples from P-wave onset.

	ROB				IMI				PCP			
	L		LPC		L		LPC		L		LPC	
	ε'_n	ε_n	ε'_n	ε_n	ε'_n	ε_n	ε'_n	ε_n	ε'_n	ε_n	ε'_n	ε_n
EGF42	0.10	0.11	0.21	0.25	0.04	0.07	0.09	0.14	0.01	0.03	0.19	0.23
EGF46	0.04	0.05	0.25	0.31	0.02	0.04	0.09	0.11	0.02	0.04	0.26	0.33
EGF48	0.04	0.05	0.17	0.19	0.03	0.05	0.23	0.25	0.02	0.03	0.26	0.30

indicates that this event had a simple rupture process (explained by the single pulse of the STF), which does not exhibit directivity. Otherwise, for MAIN5139 we observe that the widths of the source function show an azimuthal dependence, ranging from 0.055 (station ROB) to 0.120 s (station PCP). Thus we can infer that the rupture probably propagated along an approximately E–W direction. Furthermore, the rather complex shape of the STF may be due to more than one subevent in the rupture process.

In figure 12 we also give plots of the modulus of the Fourier transforms of some of the

Table 4. Same as table 3: case of MAIN5139.

	ROB				IMI				PCP			
	L		LPC		L		LPC		L		LPC	
	ε'_n	ε_n	ε'_n	ε_n	ε'_n	ε_n	ε'_n	ε_n	ε'_n	ε_n	ε'_n	ε_n
EGF42	0.02	0.05	0.16	0.19	0.03	0.04	0.10	0.13	0.01	0.02	0.36	0.43
EGF46	0.02	0.05	0.18	0.23	0.03	0.05	0.15	0.17	0.01	0.03	0.53	0.59
EGF48	0.01	0.04	0.17	0.20	0.02	0.04	0.26	0.29	0.02	0.03	0.39	0.47

Table 5. Real data analysis by means of the LPCS method. Values of the duration T of STF.

	T (ms)	
	MAIN2932	MAIN5139
PCP	45	120
ROB	50	55
IMI	50	100

restored STFs. They show that our method yields much more precise estimates of $\hat{f}(0)$, i.e. of the seismic moment, than those provided by the water-level method. For both events we computed the mean values (over all the three stations) of the seismic moment. We obtained for MAIN2932 a value of 7.0×10^{19} dyne cm^{-1} and for MAIN519 1.6×10^{20} dyne cm^{-1}. These values are consistent with the moment–magnitude relation reported in literature for the area where the swarm occurred.

Finally, in figure 13 we give an example of restoration showing that our method can also be successfully used for the analysis of quite complex events. It is very interesting to notice that in this restoration a support coinciding with the total interval containing the two events has been used. The method has given automatically zero values for the STF in the interval between the two events.

6. Concluding remarks

We have presented the application of the projected Landweber (PL) method to the estimation of the source time function (STF) of low-energy earthquakes using an empirical Green function to correct for propagation and instrumental effects. The introduction of constraints on the solution (i.e. positivity, causality and finite duration) provides estimates of the STF which are both numerically stable and physically reasonable after a relatively small number of iterations. Moreover, the constraints have avoided the unrealistic long-period trends and short-period oscillations affecting the STF obtained by means of crudely regularized deconvolution techniques (e.g. the water-level method). The validation of the PL method with numerical simulations has permitted one to calibrate the algorithm and has demonstrated that the restoration is just as precise as the deconvolution is more constrained. The constraints also allow for a not completely unreliable restoration when the deconvolution is performed using an EGF rather different from the true one. Moreover, the simulations have pointed out that a good extrapolation of the Fourier transform of the constrained STF can be achieved both at low and at high frequencies: this is evident when their spectra are

compared with those obtained with the water-level method.

In the case of real data, the relevance of this property is fundamental for a very accurate determination of seismic moment, source directivity and rupture duration. An application of this technique to some events in North-Western Italy has demonstrated the effective improvement in the analysis of the source characteristics. For example, we were able to recognize within the same seismic swarm two styles of rupture, the former simple and apparently circular (MAIN2932), the latter more complex and with evidence of unilateral propagation (MAIN5139). The application of the method to the analysis of the seismic swarm of July 1993 is in progress.

Acknowledgments

We thank P Augliera and D Spallarossa for their contribution to the computation of the hypocentre parameters of the seismic swarm of July 1993.

References

[1] Hartzell S 1978 Earthquake aftershocks as Green's functions *Geophys. Res. Lett.* **5** 1–4
[2] Joyner W B and Boore D M 1986 On simulating large earthquakes by Green's function addition of smaller earthquakes *Earthquake Source Mechanics* ed S Das *et al* (Washington, DC: American Geophysical Union) pp 269–74
[3] Kanamori H, Jennings P C, Singh S K and Astiz L 1993 Estimation of strong ground motion in Mexico City expected for large earthquakes in the Guerrero seismic gap *Bull. Seism. Soc. Am.* **83** 811–29
[4] Mueller C 1985 Source pulse enhancement by deconvolution of an empirical Green's function *Geophys. Res. Lett.* **12** 33–6
[5] Mori J and Frankel A 1990 Source parameter for small events associated with the 1986 North Palm Springs, California, earthquake determined using empirical Green's functions *Bull. Seism. Soc. Am.* **80** 278–95
[6] Velasco A, Ammon C and Lay T 1994 Empirical Green function deconvolution of broadband surface waves: rupture directivity of the 1992 Landers, California ($M_w = 7.3$) earthquake *Bull. Seism. Soc. Am.* **84** 735–50
[7] Velasco A A, Ammon C J and Lay T 1995 Source time function complexity of the Great 1989 Maquarie Ridge earthquake *J. Geophys. Res.* **100** 3989–4009
[8] Helmberger D and Wiggins R 1971 Upper mantle structure of the mid-western United States *J. Geophys. Res.* **76** 3229–45
[9] Zollo A, Capuano P and Singh S 1995 Use of small earthquake record to determine source function of a larger earthquake: an alternative method and an application *Bull. Seism. Soc. Am.* **85** 1249–56
[10] Courboulex F, Virieux J and Gibert D 1996 On the use of simulated annealing method and cross-validation theory for deconvolution of seismograms *Bull. Seism. Soc. Am.* **86** 1187–93
[11] Bertero M and De Mol C 1996 Super-resolution by data inversion *Progress in Optics* vol XXXVI, ed E Wolf (Amsterdam: Elsevier) pp 129–78
[12] Eicke B 1992 Iteration methods for convexly constrained ill-posed problems in Hilbert space *Num. Funct. Anal. Opt.* **13** 413–29
[13] Piana M and Bertero M 1997 Projected Landweber method and preconditioning *Inverse Problems* **13** 441–63
[14] Yosida K 1965 *Functional Analysis* (Berlin: Springer) p 163
[15] Bertero M 1989 Inverse and ill-posed problems *Advances in Electronics and Electron Physics* vol 75, ed P W Hawkes (New York: Academic) pp 1–120
[16] Cattaneo M and Augliera P 1990 The automatic phase-picking and event location system of the IGG Network (NW Italy) *Cahiers du Centre Européen de Géodynamique et de Séismologie* vol 1 (Luxembourg: Beffort) pp 65–74